Journal of Materials Chemistry A

Accepted Manuscript

ROYAL SOCIETY OF CHEMISTRY

www.rsc.org/materialsA

Journal Name

ARTICLE

Facile synthesis of high performance hard carbon anode materials for sodium ion batteries

Ning Sun, Huan Liu and Bin Xu*

Received 00th January 20xx,
Accepted 00th January 20xx

DOI: 10.1039/x0xx00000x

www.rsc.org/

A highly reversible, resource-abundant and low-cost anode is indispensable to the future success of sodium ion batteries (SIBs) in large-scale energy storage application. In this work, we report the facile synthesis of a biomass-derived hard carbon for SIBs by one-step pyrolysis of shaddock peel under inert atomosphere without activation or any further treatments. The pyrolytic carbon shows very high reversible sodium storage capacities up to 430.5 mAh g^{-1} at a current density of 30 mA g^{-1} and superior cycling stability with only 2.5 % capacity loss over 200 charge-discharge cycles. The high capacity, excellent cycle performance, combined with facile synthesis procedure make it a promising anode material for practical SIBs. The good Na-ion storage property of the shaddock peel-derived pyrolytic carbon is attributed to its unique honeycomb-like morphology with shortened distance for Na-ion diffusion, and the large interlayer distance which is availalbe for sodium insertion/exsersion.

Introduction

The ever-decreasing storage of non-regenerative fossil fuels and climate change have forced human beings to pay much attention to sustainable and regenerative energies and their conversion and storage. Lithium-ion batteries (LIBs) represent the state-of-the-art technology in rechargeable batteries and have been widely applied in portable electronics due to their high energy density and long cycle life[1,2]. However, the limited storage and unevenly geographical distribution of the Li element should be taken into consideration[3,4]. The large-scale production and wide-spread adoption of LIBs are expected to cause the lack of Li resources and the consequent monstrously rising price of their raw materials. Accordingly, sodium-ion batteries (SIBs) have been recently attracted growing attention as a promising commercial alternative to LIBs for large-scale and low-cost electrical energy storage application, because of the wide abundance and low cost of sodium resources[5,6,7].

One of the grand challenges for realizing SIBs is the absence of the suitable anode materials[8]. As the sodium ion has a diameter that is about 55% larger than that of the lithium ion[4], the interlayer distance of graphite (~0.34 nm) is too small to accommodate the large sodium ion. Therefore, graphite materials, the most commonly used anode materials in LIBs, show poor sodium storage capacity and are unsuitable for SIBs. The proposed anode materials include carbonaceous materials[9,10,11], alloys[12,13], metal oxides/sulfides[14,15,16] and phosphorous[17]. Na alloy anode materials have high capacity, but the large volume expansion during sodiation results in the structural destruction and thus poor cycle durability[18,19]. Therefore, amorphous hard carbons with large interlayer distance and disordered structure seem to be a promising alternative anode materials for SIBs. Theoretical calculations indicate a minimum interlayer distance of 0.37 nm is required for sodium ion insertion in the carbon[20,21]. Using sucrose[22], glucose[23] and resorcinol-formaldehyde resin[24] as precursors, hard carbons with a reversible capacity of 150-300 mAh g^{-1} have been obtained, but the cycle performance and rate capability were insufficient. Some recent reports indicate designing nanostructured morphology[20,25,26] or/and hierarchically porous structure[27,28] is an effective strategy to improve the electrochemical performance of carbon materials, as the nanostructure can provide some active sites for Na ion storage as well as decrease the diffusion distance of Na ion and enhance the rate capability. However, the developed porosity and high surface area make the initial Coulombic efficiency of these carbons very low, usually only 20-50%. Hollow carbon nanospheres[29] prepared through the hydrothermal carbonization of glucose in the presence of latex templates have delivered a reversible capacity of 160 mAh g^{-1} at 100 mA g^{-1} after 100 cycles. Wang et al[25] reported that nitrogen-doped porous carbon nanosheets with a surface area of 1477 m^2 g^{-1} can deliver a reversible capacity of 349.7 mAh g^{-1} at 50 mA g^{-1}, and retains 80 mAh g^{-1} after 400 cycles at 1A g^{-1}, but the initial Coulombic efficiency is only 34.9%. Our group have synthesized nitrogen-containing mesoporous carbons by co-pyrolyzing gelatin and magnesium citrate[30], which show a reversible sodium storage capacity of 330 mAh g^{-1} at 50 mA g^{-1} with an initial Coulombic efficiency lower than 40%. To overcome this problem, hard carbons with long-range-ordered layered structures, larger

[a] State Key Laboratory of Chemical Resource Engineering, Beijing Key Laboratory of Electrochemical Process and Technology for Materials, Beijing University of Chemical Technology, Beijing 100029, China. E-mail: binxumail@163.com; Tel/Fax: 86-10-64434907.

Electronic Supplementary Information (ESI) available: [details of any supplementary information available should be included here]. See DOI: 10.1039/x0xx00000x

interlayer distances and low porosity are desired for sodium ion storage[31].

Biomaterials, which are generally abundant, renewable, and environmentally-friendly, have been widely used as precursors for porous carbons[32,33,34]. From the green and recyclable point of view, the strategy of electrode materials synthesis using biological wastes is of great significance. What's more, the carbon will inherit the unique nature morphology, structure and properties of the biomass precursor to a certain extent. Recently, Lotfabad et al[35] prepared a biomass-derived hard carbon by the pyrolysis of banana peels at 1100 ℃ and followed air activation at 300 ℃, which delivered a reversible Na storage capacity of 355 mAh g^{-1} at 50 mA g^{-1} with good cycle performance, revealing the advantage of biomass-derived carbon as hard carbon anode materials for SIBs. Shaddocks are one of the most common fruits in Southeast Asia. The shaddock peels are not desired for consumers, and serve little economic benefits apart from being discarded as biodegradable wastes. From this view of point, shaddock peels, are an ideal precursor for value-added carbons. Besides, previous reports[36] revealed that shaddock peels contained 78% hemicellulose, 7-21% pectin, and some free sugars. The highly cross-linked and noncrystallined hemicellulose can form nongraphitic carbon at reasonable pyrolysis temperatures[35], which is just desired for our study. Hong et al[37] have prepared porous carbon with a surface area of 1272 m^2 g^{-1} from shaddock peels by H_3PO_4 activation, which delivered a reversible capacity of 314.5 mAh g^{-1} at 50 mA g^{-1} as anode for SIBs, but the initial Coulombic efficiency is only 27 %. Herein, we proposed a very simple method to prepare hard carbons for SIBs by one-step pyrolysis of shaddock peel at 800-1400 ℃ under inert atmosphere without activation or any further treatments. The unique honeycomb-like morphology and the large interlayer distance (0.38 nm) enable the pyrolytic carbon shows very high reversible sodium storage capacities up to 430 mAh g^{-1} at a constant current of 30 mA g^{-1}, with a relative high initial Coulombic efficiency of 69%. It also exhibits superior cycling stability with only 2.5 % capacity loss over 200 charge-discharge cycles at 50 mA g^{-1}. The high capacity, excellent cycle performance, combined with facile synthesis procedure make it a promising anode material for practical SIBs.

Experimental

The biomass-derived hard carbon was simply synthesized by one-step pyrolysis of shaddock peel (Scheme S1). The spongy internal capsule in the pristine shaddock peel was collected, washed with DI water, cut into small pieces, and dried at 80 ℃ for 12 h in a vacuum oven. The obtained precursor was pyrolyzed at 800-1400 ℃ for 2 h under an inert atmosphere by bubbling N_2 (99.99%) into the tubular furnace with a flow of 200 sccm min^{-1}. After ground, the pyrolysis products was washed with diluted HCl and DI water for purification, and then dried at 120 ℃ for 12 h in a vacuum oven. The carbon obtained at a pyrolysis temperature *T* is labelled as SP-*T*.

The morphology of the carbons were characterized on a scanning electron microscopy (SEM, SUPRA 55) and a transmission electron microscopy (TEM, JEOL-2100). X-ray diffraction (XRD) analysis was performed on a Bruker AXS D8 with Cu Kα radiation (λ=0.1541 nm). The Raman spectrum was recorded on Renishaw 1000 Raman spectrometer with a 50 mW He-Ne laser (514 nm) with a CCD detector. The X-ray photoelectron spectroscopy (XPS) was employed to characterize the element components of the pyrolytic carbons using a Sigma Probe spectrometer with a high performance Al monochromatic source operated at 15 KV. Fourier transformed infrared (FTIR) spectra of the pyrolytic carbons and the discharged electrodes were recorded on a Bruker VERTEX 70 V spectrometer. Nitrogen adsorption/desorption isotherms at 77 K were performed on a Micromeritics ASAP2460 to obtain pore properties such as the specific surface area, total pore volume and pore size distribution. The specific surface area (S_{BET}) was calculated by the conventional BET (Brunauer-Emmett-Teller) method. The total pore volume (V_t) was calculated from the adsorbed N_2 amount at a relative pressure of 0.99. The pore size distribution was calculated by the density function theory (DFT) method using a carbon slit pore equilibrium model.

For electrode preparation, the slurry of 80 wt% pyrolytic carbon, 10 wt% carbon black (Super-P), and 10 wt% polyvinylidene fluoride (PVDF) in N-methylpyrrolidone (NMP) were coated onto Cu foil and then dried at 120 °C for 12 h in a vacuum oven. Coin cells were assembled in an argon-filled glove box (Mikrouna, H_2O, O_2<0.1 ppm) with the prepared electrode as the working electrode, a Na foil as the counter electrode, glass fiber as the separator, and 1 mol L^{-1} $NaClO_4$ dissolved in a mixture of ethylene carbonate (EC) and diethyl carbonate (DEC) (1:1 v/v) as the electrolyte. Cyclic voltammetry (CV) was carried out using CS350 electrochemical workstation at a scan rate of 0.1 mVs^{-1}. Galvanostatic charge/discharge measurements were performed on a Land BT2000 battery tester (Wuhan, China). Electrochemical impedance spectroscopy (EIS) data were obtained using a GAMRY 07130 electrochemical workstation with an AC perturbation signal of 5 mV in the frequency range of 10^{-2}-10^5 Hz. All the electrochemical tests were conducted at room temperature.

Results and discussion

The morphology of the shaddock peel-derived pyrolytic carbon was characterized by SEM and HRTEM observation. As shown in Fig. 1a and 1b, the carbon shows honeycomb-like morphology with large cavities and thin walls, which permits the organic electrolyte to enter the "bulk" of the material and shortens the path of the sodium ions and electrons, beneficial for enhancing the performance of the material. The unique morphology of the carbons origins from inheriting the nature structure of the shaddock peel, proving the advantage of nature biomass as carbon precursors. HRTEM (Fig. 1c-f) indicates the carbons prepared at 800-1400 ℃ all show amorphous crystallites with some little graphite ribbons. The random layers in these disordered carbon materials create the sites for sodium ions insertion/extraction. Comparing the carbons prepared at different temperatures, it is found the carbon obtained at higher pyrolysis temperature shows a little more ordered

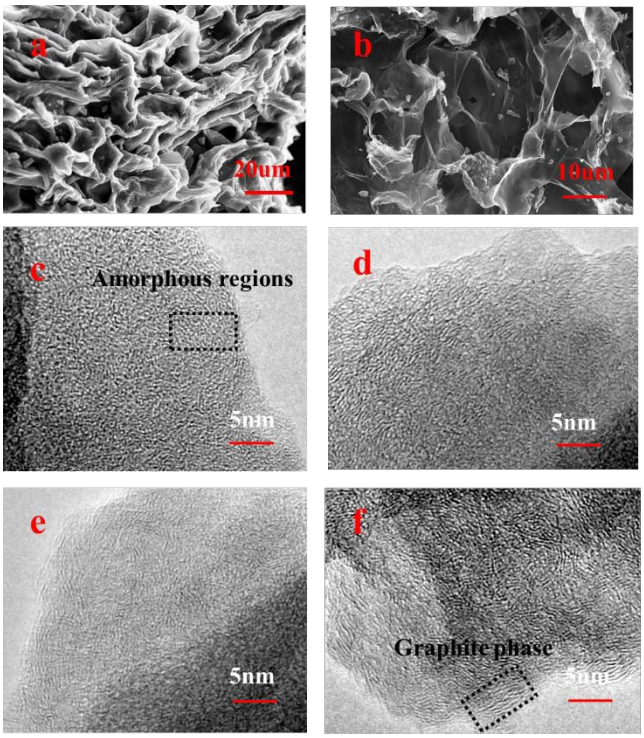

Fig. 1 SEM images of SP-800 sample at different resolution ratios (a,b) and HRTEM images of SP-800 (c), SP-1000 (d), SP-1200 (e) and SP-1400 (f).

crystallite orientation, although far from graphite.

The XRD patterns of the pyrolytic carbons prepared at different pyrolysis temperatures are shown in Fig. 2a. Two broaden diffraction peaks appear at ~22.5° and ~43.6°, corresponding to the (002) and (100) planes of graphite, confirming that the obtained carbon materials are disordered or amorphous carbons[38,39]. With the increase of the pyrolysis temperature, the gradually upshifted (002) diffraction peaks and sharpened (100) diffraction peaks suggest that carbons prepared at a higher pyrolysis temperature have a little more ordered crystalline structure, agree well with the HRTEM observation. The interlayer spacing (d002) values of the carbons calculated by Scherrer's formula based on the (002) peak is 0.376-0.392 nm (Table 1), with a decreasing tendency with pyrolysis temperature. The d002 values of all the carbons are much larger than 0.37 nm, the minimum value for Na ion insertion as predicted by theoretical calculations, implying high Na ion storage capacity can be expected.

The crystalline structure of the carbons are further characterized by Raman spectroscopy analysis. The Raman spectrum of all the carbons exhibit two broad bands of the D band peak at 1355 cm^{-1} (the disordered carbon or defective graphitic band)[38,40], and G band peak at 1590 cm^{-1} (the crystalline graphite band), characteristic of disordered structure. With pyrolysis temperature increases, both of the G and D peaks get a little sharpen, but the intensity of the I_G/I_D shows a decreasing tendency, which is in contrast to the XRD analysis and HRTEM observation. The reason is still unclear at the moment.

Tabel 1 Structure properties and Na storage performances of the shaddock peel-derived pyrolytic carbons

Sample	d_{002} (Å)	S_{BET} (m^2/g)	Vt (cm^3/g)	1st discharge/charge cycle		
				Discharge ($mAhg^{-1}$)	Charge ($mAhg^{-1}$)	Efficiency (%)
SP-800	3.92	25.5	0.010	262.8	418.6	62.8
SP-1000	3.82	68.6	0.035	314.5	499.1	63.0
SP-1200	3.80	82.8	0.049	430.5	635.9	67.7
SP-1400	3.76	39.0	0.040	359.7	520.0	69.2

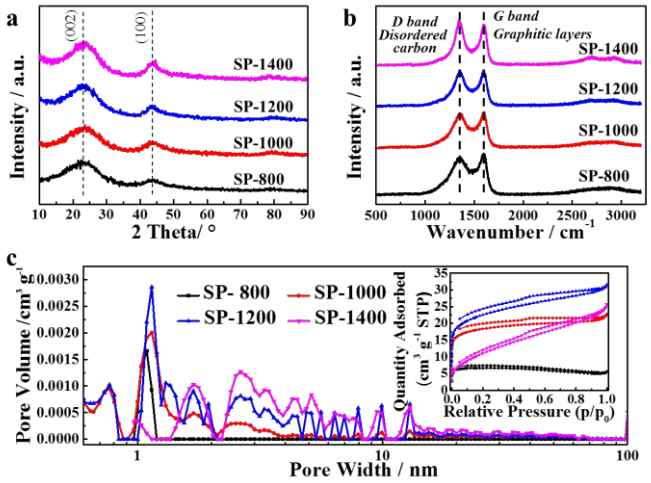

Fig. 2 (a) XRD patterns and (b) Raman spectra of the shaddock peel-derived pyrolytic carbons; (c) Pore size distribution calculated using the DFT model with the nitrogen adsorption-desorption isotherms in the inset.

X-ray photoelectron spectroscopy (XPS) analysis (Fig. S1) indicates that only a few heteroatoms (O, N) are attached on the surface of the pyrolytic carbons, which arise from the thermal stable groups in the biomass precursor. The carbon content increases gradually with the pyrolysis temperature, from 91.08 at% at 800 °C to 97.53 at% at 1400 °C while the oxygen decreases from 6.32 at% to 2.47 at% (Table S1). A little nitrogen can be detected only when the pyrolysis temperature below 1000 °C, i. e 1.97 at% and 1.29 at% for SP-800 and SP-1000, respectively.

The Nitrogen adsorption/desorption isotherms were measured to characterize the porosity structure of the carbons. Fig. 2c shows the pore size distributions of the carbons calculated using the DFT model, while the actual experimental isotherms with a type I/IV behaviour are shown in the inset. As the carbons were prepared only by direct pyrolysis of the shaddock peel at high temperature without any activation or oxidation treatment, few pores were detected in the carbons. The BET surface area of the carbons is only 25.5-82.8 $m^2 g^{-1}$ with a pore volume of 0.010-0.049 $cm^3 g^{-1}$. The pores distribute in a wide range of 0.6-15 nm. The micropores may be created by the released small hydrocarbon molecules during pyrolyzation, while the mesopores origins from the honeycomb-like structure of the shaddock peel.

Na-ion insertion-extraction behaviour in the pyrolytic carbons was evaluated by cyclic voltammetry (CV) and galvanostatic charge-discharging cycling between 0.01 and 3.0

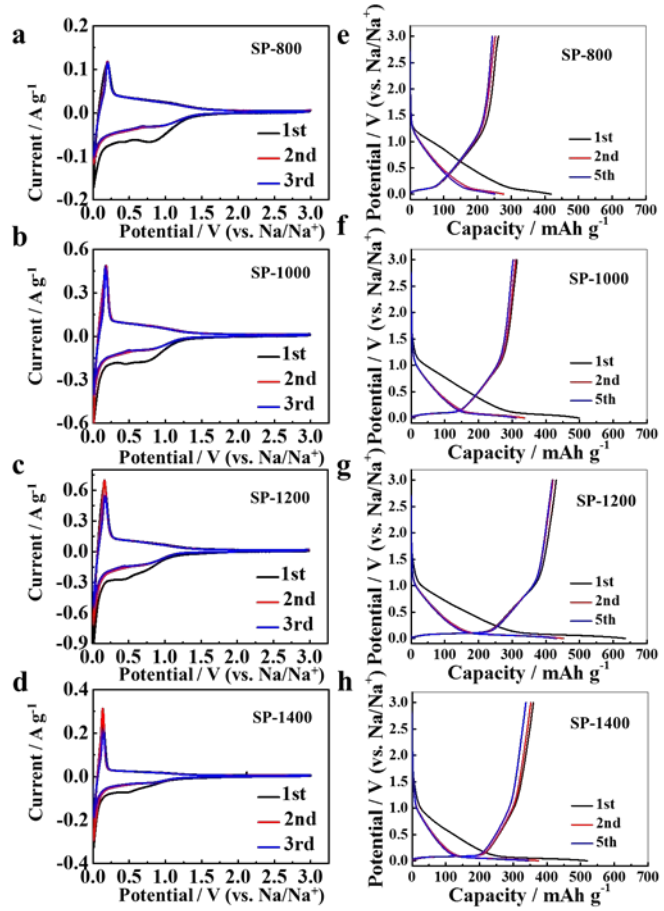

Fig. 3 Cyclic voltammograms of the pyrolytic carbons at 0.1mV s^{-1} (a-d) and charge/discharge profiles of the biomass-derived hard carbons at 30mA g^{-1} (e-h).

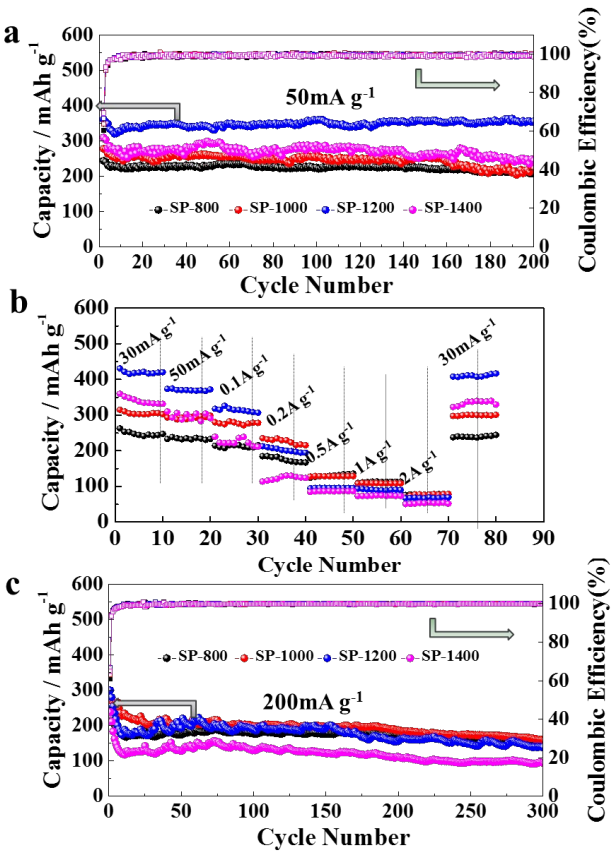

Fig. 4 Cycling performances at 50 mA g^{-1} (a), rate performance (b) and cycling performance at 200 mA g^{-1} (c) of the pyrolytic carbons.

V (vs. Na/Na^+). Fig. 3a-d shows the CV curves of the carbons in the first three cycles at a scan rate of 0.1 mV s^{-1}. Fig. 3e-h shows the galvanostatic charge-discharging profiles of the carbons in the initial cycles at a current density of 30 mA g^{-1}. The carbons obtained at different pyrolysis temperatures show very similar CV and charge-discharging behaviour in 1 M $NaClO_4$/EC+DEC. In the first reduction process, two small reduction peaks at approximately 0.5 V and 0.7 V are observed. These peaks are generally attributed to the electrolyte decomposition on the different active surfaces of the carbons and the formation of a solid electrolyte interface (SEI) film on the electrode surface[41], which are the main reasons for the initial irreversible capacity loss during the first discharge-charge cycle. In the lower potential region, a sharp pair of redox peaks appear at 0.01-0.3 V (vs. Na/Na^+). In addition, a pair of weak humps over a wide potential range of 0.2-1.0 V are observed. These pairs of sharp peaks and weak humps correspond to the plateau regions and the sloping regions of the galvanostatic charging-discharging profiles, respectively, indicating different sodium ion insertion mechanisms which will discussed below. In the subsequent cycles, both the CV curves and charging-discharging profiles almost overlap, indicating that the capacity decay mainly occurs in the first cycles, and subsequently the carbon shows good Na ion insertion-extraction reversibility and cycle stability.

The initial discharge and charge capacities of the pyrolytic carbons at 30 mA g^{-1} are listed in Table 1. With the pyrolysis temperature increases, the reversible capacity of the carbon increases from 262.8 mAh g^{-1} at 800 °C to 314.5 mAh g^{-1} at 1000 °C, and then reaches the maximum value of 430.5 mAh g^{-1} at 1200 °C, which is much higher than that of most other hard carbons, ranging from 100 to 350 mAh g^{-1} (Table S2). As the pyrolysis temperature further increases to 1400 °C, the capacity exhibit a little decrease to 359.7 mAh g^{-1}. The high capacity of the SP-1200 may be attributed to the optimized interlayer spacing (0.38 nm) and the relative developed porosity (S_{BET}: 82 m^2/g). The initial Coulombic efficiency of the pyrolytic carbons shows an increasing tendency with pyrolysis temperature and varies in 62.8-69.2%. This value is also superior to other hard carbons, especially porous and nanostructured carbons, which is generally in 20-60% (Table S2). The relative high initial Coulombic efficiency of the carbons is ascribed to their lower surface area (25.5-82.8 m^2 g^{-1}). The FTIR spectra of the pyrolytic carbon discharged to 0.0 V (Fig. S2) indicates the main components in the SEI layer are $ROCO_2Na$, Na_2CO_3 and RONa, similar to the species observed on the hard carbons.[30] Over several cycles, roughly all the absorption peaks in the electrode can find their counterparts in the initial cycle, indicating that the electrolyte decomposition and the formation of SEI mainly happened during the first charge/discharge process. Once a stable SEI layer is constructed, the Na-ion insertion/extraction is reversible, thus the columbic efficiency quickly increases to

ca.100% in the subsequently cycles. To further increase the initial Coulombic efficiency of the carbons, some strategies can be tried in future work, such as surface coating, electrolyte optimization and the use of highly effective SEI film-forming additives[20].

The cycling stabilities of the hard carbon samples during sodium insertion/extraction have been investigated at a current density of 50 mA g^{-1} in the voltage range of 0.01-3 V (vs. Na/Na^+), as displayed in Fig. 4a. The carbons prepared at different pyrolysis temperatures all exhibit good cycle stability. After 200 cycles, the sample SP-1200 retains a reversible capacity of 352 mAh g^{-1}, corresponding to a capacity retention as high as 97.5% to the 1st reversible capacity (360.9 mAh g^{-1}). After initial several to ten cycles, the Coulombic efficiency quickly increases and retains above 99% in subsequent cycles, indicating the good reversibility of the electrodes in the following cycles.

Fig. 4b displays the rate performances of the pyrolytic carbons. With the discharging/charging rate increases, the carbon prepared at lower pyrolysis temperature shows a slower capacity fading, i.e. better rate capability. However, EIS spectra (Fig. S3) indicates the carbons prepared at lower pyrolysis temperature exhibit both larger charge transfer resistance and larger electrical resistance. Similar phenomenon have also been observed[35], but the mechanism need to be further investigated. Among all the electrode samples, the SP-1200 electrode delivers the highest reversible capacities of 430.5, 373.5, 317.7 $mAhg^{-1}$ at 30 mA g^{-1}, 50 mA g^{-1} and 100 mA g^{-1}, respectively. Although the SP-800 can only delivers a reversible capacity of 262.8 mAh g^{-1} at 30 mA g^{-1}, it shows the best rate capability. As the current density increases to 2 A g^{-1}, a capacity of 78.3 $mAhg^{-1}$ can still be retained in the SP-800 electrode, which is very close to that of SP-1000 and SP-1200. The good rate performance of the pyrolytic carbon may be attributed to the honeycomb-like morphology which shortened the diffusion path of the Na^+, as well as the large interlayer distance, beneficial for the Na ion insertion and extraction. The pyrolytic carbons also shows good cycling performance at large current densities (Fig. 4c and S4). For example, the SP-1000 can afford a capacity of 158.9 mAh g^{-1} after 300 cycles at 200 mA g^{-1}, and 100.4 mAh g^{-1} after 500 cycles at 500 mA g^{-1}.

The charge storage mechanism of sodium in carbon materials remains unclear, with no consensus in the literature[42]. The proposed mechanisms include chemisorption on surface heteroatoms[43], metal nanopore filling[20,23], intercalation between graphene layers[41,44], and reversible adsorption at structural defect sites and pore surface[30,45]. As shown in Fig. 5a, the shaddock peel-derived carbons prepared at different pyrolysis temperatures display similar voltage profiles at 30 mAg^{-1}, composed of a sloping-voltage region and a nearly plateau at potentials lower than 0.2 V, all characteristic of the behaviour of the hard carbon anode materials. According to the previous reports[20,35,39,42], the reaction occurring at higher potential (0.2−1V) range is attributed to the charge transfer on the surface of small graphitic clusters or surface electro-adsorption/desorption, while the reaction occurring at the narrow low potential range (0−0.2 V) is ascribed to Na-ion insertion−extraction in the interlayer of the graphitic crystallites as illustrated in Fig. S3. To quantitatively distinguish the contribution of the two charge storage mechanisms, the total capacities are divided into two portions, the fraction associated with the plateau region below 0.1 V and sloping region above 0.1 V, which are summarized in the histogram shown in Fig. 5e-h. At a low rate of 30 mAg^{-1}, the sub-0.1 V capacities shows an increasing tendency with the pyrolysis temperature, being 81.1 mAh g^{-1} for SP-800, 148.8 mAh g^{-1} for SP-1000, 254.4 mAh g^{-1} for SP-1200, and 218.9 mAh g^{-1} for SP-1400, while the high-voltage capacity above 0.1 V is independent to the pyrolysis temperature. It seems sodium ions are more likely to insert into the graphene layers with the increase of the structural order and the gradual reduce of defects.

To further investigate the electrochemical behaviour of the carbons at enhanced current density, the voltage profile of the carbons at different rates and the separate capacities of plateau region and sloping region are also presented in Fig. 5 and Fig. S5. The charging-discharging profiles of the carbons at the current density below 200 mA g^{-1} all show a monotonous sloping region and a plateau region at lower potential. However, as the current density increases above 500 mA g^{-1}, the plateau region disappears and only a sloping region is observed, indicating surface charge transfer or surface electro-adsorption/desorption mechanism is predominate for charge

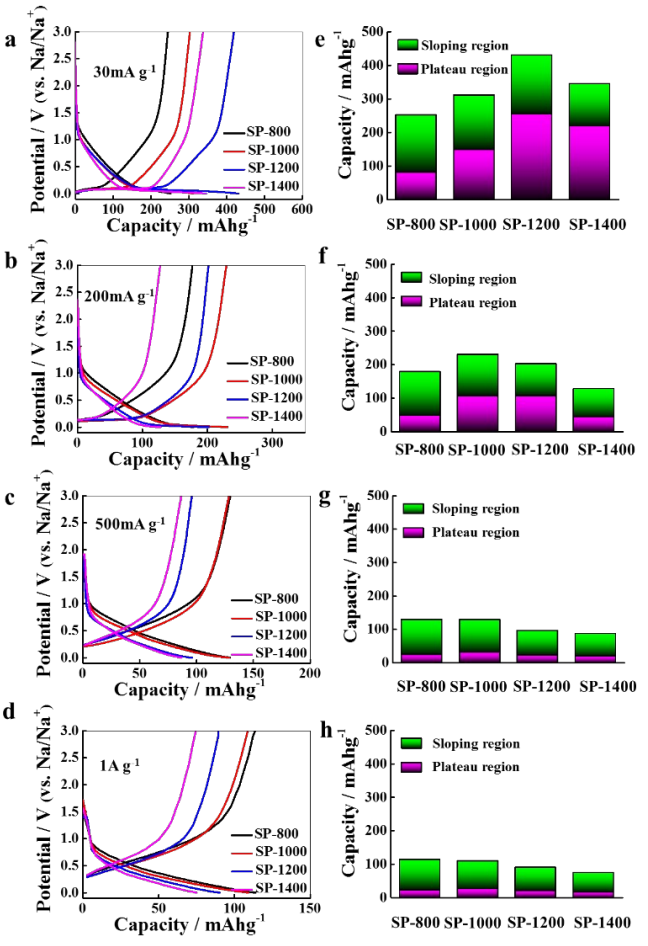

Fig. 5 Charge/discharge profiles (a-d) and summery of capacity above and below 0.1 V in the pyrolytic carbons (e-h), 5th cycle at different current density.

storage. Quantitative analysis indicates although both the sloping capacities and plateau capacities gradually decreases with the current density, the sloping capacities exhibit much better rate durability than the plateau capacities (Fig. S6). For instance, as the current density increases to 1 A g^{-1}, the sloping capacity of SP-1000 (83.3 mA g^{-1}) retains 51 % of that at 30 mA g^{-1} (162.7 mAh g^{-1}), while its plateau capacity decreases from 148.8 mA g^{-1} to 25.8 mA g^{-1}, only 17% retained. It is obvious that the insertion/extraction of Na-ion in the interlayer of the carbons is dynamically much slowly than the adsorption/desorption of Na-ion on defects or pores of the carbons.

A comparison of the performance of SP-1200 with state-of-the-art carbons is presented in Table S2. Carbons included in the comparison are carbon microsphere, template mesoporous carbon, carbon nanofiber, hollow carbon nanowire, graphene, and hard carbons derived from resin, sucrose and biomass. From Table S2, it can been seen that the overall performance of SP-1200 specimen are quite favourable in terms of both reversible capacity (430.5 mAh g^{-1} at 30 mA g^{-1}) and cycling stability (2.5 % capacity loss over 200 charge-discharge cycles). What's more, the nanostructured /porous carbons are usually synthesized by well-designed strategy, which is mostly complicated, tedious, costly and difficult for large scale production. However, for the present method, the carbon precursor is biomass waste, and the preparing process is very simple, only involving a direct pyrolysis process. It is concluded that the present method is promising to prepare highly reversible, resource-abundant and low-cost anode carbon materials for practical SIBs.

Conclusion

A highly reversible, resource-abundant and low-cost anode carbon materials were simply prepared from biomass waste by direct pyrolysis of shaddock peel without activation or any further treatments. Thanks to the honeycomb-like morphology and the large interlayer distance, the pyrolytic carbon shows a high reversible capacity of 430.5 mAh g^{-1} with excellent cycling performance. Combined with the facile synthesis procedure and sustainable resource, the present biomass-based pyrolytic carbon may be a promising anode material for practical SIBs. The present work also gives a new insight for the high value-added usage of biomass wastes. Inspired by this strategy, a series hard carbons could be simply prepared from other biomass.

Acknowledgements

This work was financially supported by the National Key Basic Research and Development Program (2015CB251100) and the National Science Foundation of China (51572011, 21073233).

Notes and References

1 J. B. Goodenough and K. S. Park, *Journal of the American Chemical Society*, 2013, **135**, 1167.
2 B. Scrosati, J. Hassoun,Y.-K. Sun, *Energy & Environmental Science*, 2011, **4**, 3287.
3 H. L. Pan, Y. S. Hu and L. Q. Chen, *Energy & Environmental Science*, 2013, **6**, 2338.
4 S. Y. Hong, Y. Kim, Y. Park, A. Choi, N. S. Choi and K. T. Lee, *Energy & Environmental Science*, 2013, **6**, 2067.
5 L. P. Wang, L. H. Yu, X. Wang, M. Srinivasan and Z. C. J. Xu, *Journal of Materials Chemistry A*, 2015, **3**, 9353.
6 V. Palomares, M. Casas-Cabanas, E. Castillo-Martínez, M. H. Han and T. Rojo, *Energy & Environmental Science*, 2013, **6**, 2312.
7 C. Nithya and S. Gopukumar, *Wiley Interdisciplinary Reviews: Energy and Environment*, 2015, **4**, 253.
8 M. Dahbi, N. Yabuuchi, K. Kubota, K. Tokiwa and S. Komaba, *Physical Chemistry Chemical Physics*, 2014, **16**, 15007.
9 Y. Yan, Y. X. Yin, Y. G. Guo and L. J. Wan, *Advanced Energy Materials*, 2014, **4**, 1301584.
10 Y. Li, S. Xu, X. Wu, J. Yu, Y. Wang, Y.-S. Hu, H. Li, L. Chen and X. Huang, *J. Mater. Chem. A*, 2015, **3**, 71.
11 J. Xu, M. Wang, N. P. Wickramaratne, M. Jaroniec, S. Dou and L. Dai, *Advanced Materials*, 2015, **27**, 2042.
12 J. Liu, Y. Wen, P. A. van Aken, J. Maier and Y. Yu, *Nano letters*, 2014, **14**, 6387.
13 A. Darwiche, M. Toiron, M. T. Sougrati, B. Fraisse, L. Stievano and L. Monconduit, *Journal of Power Sources*, 2015, **280**, 588.
14 Y. Cao, L. Xiao, W. Wang, D. Choi, Z. Nie, J. Yu, L. V. Saraf, Z. Yang and J. Liu, *Advanced Materials*, 2011, **23**, 3155.
15 J.-W. Wen, D.-W. Zhang, Y. Zang, X. Sun, B. Cheng, C.-X. Ding, Y. Yu and C.-H. Chen, *Electrochimica Acta*, 2014, **132**, 193.
16 D. Y. Yu, P. V. Prikhodchenko, C. W. Mason, S. K. Batabyal, J. Gun, S. Sladkevich, A. G. Medvedev and O. Lev, *Nature Communications*, 2013, **4**, 2922.
17 Y. Zhu, Y. Wen, X. Fan, T. Gao, F. Han, C. Luo, S. C. Liou and C. Wang, *ACS Nano*, 2015, **9**, 3254.
18 I. T. Kim, E. Allcorn and A. Manthiram, *Journal of Power Sources*, 2015, **281**, 11.
19 V. Palomares, P. Serras, I. Villaluenga, K. B. Hueso, J. Carretero-Gonzalez and T. Rojo, *Energy & Environmental Science*, 2012, **5**, 5884.
20 Y. Cao, L. Xiao, M. L. Sushko, W. Wang, B. Schwenzer, J. Xiao, Z. Nie, L. V. Saraf, Z. Yang and J. Liu, *Nano letters*, 2012, **12**, 3783.
21 C. Bommier, W. Luo, W.-Y. Gao, A. Greaney, S. Ma and X. Ji, *Carbon*, 2014, **76**, 165.
22 T. Chen, L. Pan, T. Lu, C. Fu, D. H. C. Chua and Z. Sun, *J. Mater. Chem. A*, 2014, **2**, 1263.
23 D. A. Stevens and J. R. Dahn, *Journal of The Electrochemical Society*, 2000, **147**, 1271.
24 J. Liu, H. Liu, T. Yang, G. Wang and M. O. Tade, *Chinese Science Bulletin*, 2014, **59**, 2186.
25 H. G. Wang, Z. Wu, F. L. Meng, D. L. Ma, X. L. Huang, L. M. Wang and X. B. Zhang, *ChemSusChem*, 2013, **6**, 56.
26 L. Fu, K. Tang, K. Song, P. A. van Aken, Y. Yu and J. Maier, *Nanoscale*, 2014, **6**, 1384.
27 S. Wenzel, T. Hara, J. Janek and P. Adelhelm, *Energy & Environmental Science*, 2011, **4**, 3342.
28 H. Song, N. Li, H. Cui and C. Wang, *Nano Energy*, 2014, **4**, 81.
29 K. Tang, L. Fu, R. J. White, L. Yu, M.-M. Titirici, M. Antonietti and J. Maier, *Advanced Energy Materials*, 2012, **2**, 873.
30 Z. Guan, H. Liu, B. Xu, X. Hao, Z. Wang and L. Chen, *J. Mater. Chem. A*, 2015, **3**, 7849.
31 Y. Wen, K. He, Y. Zhu, F. Han, Y. Xu, I. Matsuda, Y. Ishii, J. Cumings and C. Wang, *Nature Communications*, 2014, **5**, 4033.
32 B. Xu, S. Hou, G. Cao, F. Wu and Y. Yang, *Journal of Materials Chemistry*, 2012, **22**, 19088.

33 M. Biswal, A. Banerjee, M. Deo and S. Ogale, *Energy & Environmental Science*, 2013, **6**, 1249.
34 Z. Li, W. Lv, C. Zhang, B. Li, F. Kang and Q.-H. Yang, *Carbon*, 2015, **92**, 11.
35 E. M. Lotfabad, J. Ding, K. Cui, A. Kohandehghan, W. P. Kalisvaart, M. Hazelton and D. Mitlin, *ACS Nano*, 2014, **8**, 7115.
36 Y. Wandee, D. Uttapap, S. Puncha-arnon, C. Puttanlek, V. Rungsardthong and N. Wetprasit, *International Journal of Food Science & Technology*, 2014, **49**, 2348.
37 K. L. Hong, L. Qie, R. Zeng, Z. Q. Yi, W. Zhang, D. Wang, W. Yin, C. Wu, Q. J. Fan, W. X. Zhang and Y. H. Huang, *Journal of Materials Chemistry A*, 2014, **2**, 12733.
38 W. Luo, J. Schardt, C. Bommier, B. Wang, J. Razink, J. Simonsen and X. L. Ji, *Journal of Materials Chemistry A*, 2013, **1**, 10662.
39 X. Zhou and Y.-G. Guo, *ChemElectroChem*, 2014, **1**, 83.
40 P. Lian, X. Zhu, S. Liang, Z. Li, W. Yang and H. Wang, *Electrochimica Acta*, 2010, **55**, 3909.
41 S. Komaba, W. Murata, T. Ishikawa, N. Yabuuchi, T. Ozeki, T. Nakayama, A. Ogata, K. Gotoh and K. Fujiwara, *Advanced Functional Materials*, 2011, **21**, 3859.
42 X.-F. Luo, C.-H. Yang, Y.-Y. Peng, N.-W. Pu, M.-D. Ger, C.-T. Hsieh and J.-K. Chang, *J. Mater. Chem. A*, 2015, **3**, 10320.
43 Z. Wang, L. Qie, L. Yuan, W. Zhang, X. Hu and Y. Huang, *Carbon*, 2013, **55**, 328.
44 H. J. Ding, Z. Li, A. Kohandehghan, K. Cui, Z. Xu,, *ACS Nano*, 2013, **7**, 11104.
45 D. Datta, J. Li and V. B. Shenoy, *ACS Applied Materials & Interfaces*, 2014, **6**, 1788.

Graphical Abstract

Hard carbon materials with high reversible sodium storage capacities up to 430.5 mAh g^{-1} and superior cycling stability were simply synthesized by one-step pyrolysis of shaddock peel for sodium-ion batteries.